SUPPORTING INFORMATION

for

Structural Insights into α-Synuclein Fibril Polymorphism: Effects of Parkinson's Disease Related C-Terminal Truncations

X. Ni, R.P. McGlinchey, J. Jiang, and J.C. Lee

MATERIAL AND METHODS

Reagents. Chemicals were obtained from Sigma unless otherwise noted.

Protein expression and purification. Plasmids for C-terminally truncated α-syn variants (residues 1–122 and 1–103) were constructed using the QuikChange site-directed mutagenesis kit (Agilent) through the insertion of a stop codon at the desired locations into the pRK172 plasmid.[1] The full length protein contains a silent mutation (TAT) at residue 136 to avoid the spontaneous mutation of Tyr-to-Cys.[2] Constructs were verified by DNA sequencing (Macrogen USA). Acetylation (Ac) of the N-termini of full-length Ac1–140 and C-terminally truncated α-syn (Ac1–122 and Ac1–103) were achieved by co-expressing pNatB[3] as previously described.[4] Purification of Ac1–140 and Ac1–122 were carried out similarly as previously described[5] with minor modifications. Steps of freeze/thaw cycles and sonication was performed prior to heat treatment. The running buffer for anionic exchange chromatography (DEAE and MonoQ) was pH 8 and 9 (20 mM Tris) for Ac1–140 and Ac1–122, respectively. Since Ac1–103 has a significant higher p*I*, a different protocol was used. Briefly, cells were resuspended in lysis buffer (100 mM Tris, 300 mM NaCl, 1 mM EDTA, pH 8.0 supplemented with protease inhibitor tablets (Roche)), followed by 2 freeze/thaw cycles (dry ice and 37 °C water bath), and probe-tip sonication on ice (Branson 450, output 4, 50% duty cycle, 4–15 min). The cellular debris were removed by centrifugation (Sorval SS34, 18,000 rpm for 30 min, 4 °C). The supernatant was then titrated to pH 3.5 by the addition of concentrated HCl, stirred for 10 min at 4 °C, and separated from insoluble materials by centrifugation (Sorval SS34, 18,000 rpm for 30 min, 4 °C). Following dialysis into a low salt buffer (20 mM 2-(N-morpholino)ethanesulfonic acid (MES), pH 6), the protein was then applied to a HiPrep SP column (GE Healthcare) and eluted with a linear salt gradient (in the range of 75–100 mM NaCl). Fractions containing Ac1–103 was subjected to another round of cationic exchange chromatography (MonoS column 10/100, GE Healthcare, equilibrated in 20 mM MES, pH 6 buffer). The protein eluted in the range of ~ 40–90 mM NaCl. All steps were carried out at 4 °C. Sample homogeneity and identity were evaluated using SDS-PAGE visualized by silver staining and LC-MS (NHLBI Biochemistry Core). Measured masses were 14,502, 12,383, and 10,346 Da for Ac1–140, Ac1–122, and Ac1–103. Based on MS, all α-syn variants was 100% acetylated with a minor population (~5%) of methionine-oxidized species. Protein concentrations were determined using a molar extinction coefficient estimated on basis of amino-acid content: $\varepsilon_{280\ nm}$ = 5,120 M^{-1} cm^{-1} for Ac1–140 and 1490 M^{-1} cm^{-1} for Ac1–122 and Ac1–103. All purified proteins were aliquoted and stored at −80 °C until use. All buffers were filtered (0.22 μm).

Fibril formation and ThT kinetics. Prior to aggregation, protein samples were exchanged into pH 7.4 buffer (10 mM NaPi, 140 mM NaCl) using a PD-10 column (GE Healthcare) and filtered through YM-100 spin units (Millipore) to remove any preformed aggregates. For cryoEM studies, fibrils were formed by aggregating Ac1–140, Ac1–122, and Ac1–103 in microcentrifuge tubes (cat. 022431081, Eppendorf) containing 1 mL solution (100–300 μM) with continuous shaking at 600 rpm at 37 °C for 4–5 days in a Mini-Micro 980140 shaker (VWR). Fibrils were stored at RT

until use. For ThT (10 μM) monitored aggregation of Ac1–140, Ac1–122 and Ac1–103, reactions (40 μL, 50 μM) were carried out in sealed black, polypropylene, 384-well flat-bottom microplates (781209, Greiner Bio-one) supplemented with a 2-mm glass bead. Seeds (Ac1–140 or Ac1–103) were added (1 μL from aggregation reactions performed at 100 μM as described above) to a solution of [α-syn] = 50 μM to a final volume of 40 μL. Fluorescence (excited and monitored at 415 and 480 nm, respectively) was recorded at 37 °C with continuous linear shaking (1 mm) using a microplate reader (Tecan Infinite M200 Pro). A total of 2 independent experiments was performed with at least 4 replicates on each plate. ThT was not added to samples used for Raman measurements.

TEM. Samples (10 μL) were applied to TEM grids (400-mesh formvar and carbon coated copper, Electron Microscopy Sciences) for approx. 2 min and wicked away by filter paper. Addition of 10 μL of deionized water was then applied and wicked away immediately. A solution of 1% uranyl acetate (10 μL) is placed on the grid for 2 min, wicked away, and air-dried. TEM was performed using a JEOL JEM 1200EX transmission electron microscope (accelerating voltage 80 keV) equipped with an AMT XR-60 digital camera (NHLBI EM Core Facility). Fibril helical twists were calculated using the image processing package, Fiji.

Raman spectroscopy. Aggregated samples were centrifuged for 30 min at 17,000 *g* prior to deposition (4 μL) on round quartz cover slips (25-mm diameter, Electron Microscopy). Data were collected at RT using 514 nm excitation (~ 65 mW at the sample) from an Ar-ion laser (CVI Melles Griot, 35-MAP-431-200) and a 60× water immersion objective (Olympus, UPLSAPO60XW) on a home-built Raman microscope as previously described.[6] A pinhole (400-μm, Thorlabs) at the imaging plane before the spectrometer (Horiba Scientific, iHR 320)) was used and pixels 120–146 in the *y*-direction of the CCD array (Horiba Scientific, Symphony II) were binned. Spectra were averages of at least 2 different spatial locations with each collection consists of 30 accumulations (8-s integration time) from 500–3700 cm^{-1}. At least 2 independent aggregated samples have been measured. Spectra were corrected by subtracting buffer background and applying a baseline polynomial fit (LabSpec 6 software, Horiba Scientific). For comparison, the maxima of the amide I bands (1669 cm^{-1}) were normalized.

Degradation reactions of α-Syn fibrils. In glass vials, Ac1–140, Ac1–122 and Ac 1–103 (50 μM) was incubated with Proteinase K (Invitrogen) (4, 0.8 and 0.4 ng total) or GluC (New England Biolabs) (3.33, 0.66 and 0.33 μg total) in reaction buffer (10 mM NaPi, 140 mM NaCl, pH 7.4) in a total volume of 25 μL for Proteinase K and 30 μL for GluC. For GluC reaction, a 2X supplied reaction buffer was also used. Samples were agitated at 600 rpm for 20 h at 37 ^{o}C in a Mini-Micro 980140 shaker (VWR). Reactions were terminated with 0.1% TFA and 3 M guanidinium hydrochloride.

LC-MS. Proteolyzed samples (5 μL) were separated using a HPLC (Agilent 1100 series HPLC, Agilent Technologies) on a reverse phase C18 column (Zorbax, 2.1 x 50mm, 3.5μm, Agilent Technologies). Intact protein (peptides) masses of α-syn were obtained with an Agilent 6224 electrospray ionization time-of-flight LC-MS. For mobile phase, a gradient (0–50% acetonitrile and 0.05% TFA) at a flow rate of 0.2 mL/min was used. The HPLC systems and MSD were controlled and data analyzed using the Agilent MassHunter Workstation platform.

CryoEM specimen preparation and data collection. Ac1–140 fibril solution (3 μL) was directly applied to freshly glow-discharged holey carbon grid (Quantifoil R1.2/1.3, copper, 300 mesh). For Ac1–122 and Ac1–103 fibrils, samples were spun down and washed twice in reaction buffer prior to use. The grids were blotted for 7 s and plunge frozen in liquid nitrogen-cooled liquid ethane using FEI Vitrobot Mark IV machine. Data were collected on a Titan Krios G3 electron microscope

(Thermo-Fisher) operated at 300 kV and equipped with a Gatan Quantum LS imaging energy filter (GIF, energy filter slit width was set at 20 eV). Images were acquired on a K2 Summit direct detection camera at a magnification of 130,000*x* using Leginon[7] software package automatically. Dose fractionations with 50 frames in super-resolution mode were recorded for 10 s exposure with a total dose of ~69 electrons per square angstrom ($e^-/Å^2$) for each micrograph. Detailed data collection parameters are listed in Table S3.

CryoEM data processing. MotionCorr2[8] was used to perform a beam-induced motion correction and dose weighting in two folds binning images with a resulting pixel size of 1.06 Å. CTFFIND4[9] was used to estimate defocus parameters. The following 2D classification, 3D classification, and 3D refinement were performed using RELION 3.0.[10 10b]

Filament segments were manually picked and extracted using a box size of 200 pixels and an inter-box distance of 27 pixels (center-to-center). For the full length Ac1–140 sample, a total of 12,132 segments with 183,065 particles were extracted from 429 selected micrographs. A total of 10,202 segments with 107,071 particles were extracted from 322 selected micrographs for Ac1-122, while 158,687 particles from 15,504 segments were extracted from 612 selected micrographs for Ac1-103 sample (Table S3). 2D classification was carried out with the regularisation parameter T = 10, and 2D class averages with a clear separation of β-strands were selected for further 3D reconstructions.

Power spectra of 2D class averages show a strong layer line at 4.8 Å that corresponds to the helical rise (Figure. S4). From the 2D class averages , we observed two filaments taking a staggered conformation for all three fibril segments. This is consistent with an approximate 2_1 screw symmetry between two protofilaments of α-syn subunits. Therefore, the helical rise between two protofilaments is 4.8 Å / 2 = 2.4 Å (Figure S6). An additional 2D classification was performed with segments extracted from a very large box size (1500 pixels) to determine the approximate pitches of the three α-syn fibrils. Considering the image features are repeated at a distance of half pitch, by measuring the distance between two adjacent repeats we got the length of half pitch. The initial helical twists were calculated from these pitches with the above deducted helical rise.

The initial 3D classification was performed using a cylinder generated *via* the relion helix_toolbox and low-pass filter to 60 Å as the initial model. 3D classification was started with a single class (K=1) with the regularization parameter T = 20 and a central Z length of 10%, which defines the central part of the helical reconstruction. The resulting density map was used as reference for further 3D classifications with 6 classes. For the reconstruction of Ac1–140, 18,397 particles were selected through the 3D classifications and subjected to the final 3D refinement with optimized helical symmetry, while 48,236 and 37,364 particles were selected for the final 3D refinement for Ac1–122 and Ac1–103, respectively. The final helical twist was optimized to 179.643° for Ac1–140, 179.473° for Ac1–122 and 179.321° for Ac1–103 (Table S3). When the 2_1 screw symmetry is not applied, the twist angle is −0.714° for Ac1-140, −1.054° for Ac1-122, and −1.358° for Ac1-103 (Figure 2D). Post-processing was carried out with a soft-edge mask and an estimated sharpening B-factor of −80 $Å^2$ for Ac1–140 and Ac1–122, and −100 $Å^2$ for Ac1–103. CTF refinement and Bayesian polishing were performed before the final post-processing step using RELION 3.0. The overall resolution was reported at 2.8, 3.0 and 3.4 Å for Ac1–140, Ac1–122, and Ac1–103, respectively (by the FSC 0.143 criterion). The local resolution was estimated in RELION 3.0. The three structures reported here have a conserved core structure similar to that of the available cryoEM structures of α-synuclein fibrils.[11] All these structures are left-handed helices, consistent with previously reported results from atomic force microscopy analysis.[11c]

Model building and refinement

The atomic models of α-syn fibrils (Ac1–140, Ac1–122 and Ac1–103) were manually built in COOT[12] from scratch. The high-quality EM maps allowed us to unambiguously build residues V37–K97, Y39–K97, Y39–V95 for Ac1–140, Ac1–122, and Ac1–103, respectively. The resulting models (10 monomers with 5 adjacent layers) were refined against the EM maps using the real space refinement in PHENIX.[13] The statistics are summarized in Table S3.

Accession codes

The cryoEM density maps for all three α-Syn fibrils (Ac1-140, Ac1-122, and Ac1-103) were deposited in the Electron Microscopy Data Bank with the accession number EMD-20183, EMD-20185 and EMD-20186 respectively. The associated atomic models were deposited in the RCSB Protein Data Bank with the entry code 6OSJ, 6OSL and 6OSM respectively.

(1) Jakes, R.; Spillantini, M. G.; Goedert, M., Identification of 2 distinct synucleins from human brain. *FEBS Lett.* **1994,** *345*, 27-32.
(2) Masuda, M.; Dohmae, N.; Nonaka, T.; Oikawa, T.; Hisanaga, S. I.; Goedert, M.; Hasegawa, M., Cysteine misincorporation in bacterially expressed human α-synuclein. *FEBS Lett.* **2006,** *580*, 1775-1779.
(3) Johnson, M.; Coulton, A. T.; Geeves, M. A.; Mulvihill, D. P., Targeted amino-terminal acetylation of recombinant proteins in E. Coli. *PLoS One* **2010,** *5*, 5.
(4) O'Leary, E. I.; Jiang, Z. P.; Strub, M. P.; Lee, J. C., Effects of phosphatidylcholine membrane fluidity on the conformation and aggregation of N-terminally acetylated α-synuclein. *J. Biol. Chem.* **2018,** *293*, 11195-11205.
(5) Pfefferkorn, C. M.; Lee, J. C., Tryptophan probes at the α-synuclein and membrane interface. *J. Phys. Chem. B* **2010,** *114*, 4615-4622.
(6) Flynn, J. D.; McGlinchey, R. P.; Walker, R. L.; Lee, J. C., Structural features of α-synuclein amyloid fibrils revealed by Raman spectroscopy. *J. Biol. Chem.* **2018,** *293*, 767-776.
(7) Suloway, C.; Pulokas, J.; Fellmann, D.; Cheng, A.; Guerra, F.; Quispe, J.; Stagg, S.; Potter, C. S.; Carragher, B., Automated molecular microscopy: The new leginon system. *J. Struct. Biol.* **2005,** *151*, 41-60.
(8) Zheng, S. Q.; Palovcak, E.; Armache, J. P.; Verba, K. A.; Cheng, Y. F.; Agard, D. A., Motioncor2: Anisotropic correction of beam-induced motion for improved cryo-electron microscopy. *Nat. Methods* **2017,** *14*, 331-332.
(9) Rohou, A.; Grigorieff, N., Ctffind4: Fast and accurate defocus estimation from electron micrographs. *J. Struct. Biol.* **2015,** *192*, 216-221.
(10) (a) Zivanov, J.; Nakane, T.; Forsberg, B. O.; Kimanius, D.; Hagen, W. J. H.; Lindahl, E.; Scheres, S. H. W., New tools for automated high-resolution cryo-em structure determination in Relion-3. *eLife* **2018,** *7*, 22. (b) Scheres, S. H. W., Relion: Implementation of a bayesian approach to cryo-em structure determination. *J. Struct. Biol.* **2012,** *180*, 519-530.
(11) (a) Guerrero-Ferreira, R.; Taylor, N. M. I.; Mona, D.; Ringler, P.; Lauer, M. E.; Riek, R.; Britschgi, M.; Stahlberg, H., Cryo-em structure of α-synuclein fibrils. *eLife* **2018,** *7*, 18. (b) Li, B. S.; Ge, P.; Murray, K. A.; Sheth, P.; Zhang, M.; Nair, G.; Sawaya, M. R.; Shin, W. S.; Boyer, D. R.; Ye, S. L.; Eisenberg, D. S.; Zhou, Z. H.; Jiang, L., Cryo-em of full-length α-synuclein reveals fibril polymorphs with a common structural kernel. *Nat. Commun.* **2018,** *9*, 10. (c) Li, Y. W.; Zhao, C. Y.; Luo, F.; Liu, Z. Y.; Gui, X. R.; Luo, Z. P.; Zhang, X.; Li, D.; Liu, C.; Li, X. M., Amyloid fibril structure of α-synuclein determined by cryoelectron microscopy. *Cell Res.* **2018,** *28*, 897-903.
(12) Emsley, P.; Cowtan, K., Coot: Model-building tools for molecular graphics. *Acta Crystallogr. Sect. D-Biol. Crystallogr.* **2004,** *60*, 2126-2132.
(13) Adams, P. D.; Afonine, P. V.; Bunkoczi, G.; Chen, V. B.; Davis, I. W.; Echols, N.; Headd, J. J.; Hung, L. W.; Kapral, G. J.; Grosse-Kunstleve, R. W.; McCoy, A. J.; Moriarty, N. W.; Oeffner, R.; Read, R. J.; Richardson, D. C.; Richardson, J. S.; Terwilliger, T. C.; Zwart, P. H., Phenix: A comprehensive python-based system for macromolecular structure solution. *Acta Crystallogr. Sect. D-Biol. Crystallogr.* **2010,** *66*, 213-221.

Table S1. MS analysis of PK digestion of Ac1–140, Ac1–122, and Ac1–103 fibrils.

Ac1–140$_f$ (40 μM) +Proteinase K (4 ng)

Observed Mass (Da)	Theoretical Mass (Da)	Position in α-syn sequence
8010.15	8010.05	29–109
7868.01	7867.89	31–109
7256.44	7256.28	31–103

Ac1-140$_f$ (40 μM) +Proteinase K (0.4 ng)

Observed Mass (Da)	Theoretical Mass (Da)	Position in α-syn sequence
14502.28	14502.16	1–140
8010.15	8010.05	29–109
7868.01	7867.89	31–109
7256.44	7256.28	31–103

Ac1–122$_f$ (40 μM) +Proteinase K (4 ng)

Observed Mass (Da)	Theoretical Mass (Da)	Position in α-syn sequence
9123.60	9123.29	18–109
7256.54	7256.28	31–103

Ac1-122$_f$ (40 μM) +Proteinase K (0.4 ng)

Observed Mass (Da)	Theoretical Mass (Da)	Position in α-syn sequence
12383.07	12383.00	1–122
10548.87	10548.82	18–122
9993.82	9993.30	9–109
9535.92	9535.77	18–113
9123.46	9123.29	18–109

Ac1-103$_f$ (40 μM) +Proteinase K (4 ng)

Observed Mass (Da)	Theoretical Mass (Da)	Position in α-syn sequence
10346.30	10345.86	1–103
9811.34	9811.27	5–103
9551.89	9551.91	7–103
9381.94	9381.69	9–103
7256.37	7256.28	31–103

Ac1–103$_f$ (40 μM) +Proteinase K (0.4 ng)

Observed Mass (Da)	Theoretical Mass (Da)	Position in α-syn sequence
10346.94	10345.86	1–103
9811.29	9811.27	5–103
9382.02	9381.69	9–103
7256.38	7256.28	31-103

Table S2. MS analysis of GluC digestion of Ac1–140, Ac1–122 and Ac1–103 fibrils.

Ac1–140$_f$ (40 μM) +GluC (3.33 μg)

Observed Mass (Da)	Theoretical Mass (Da)	Position in α-syn sequence
14502.45	14502.16	1–140
11554.94	11554.74	29–140
9565.23	9564.70	29–123

Ac1–140$_f$ (40 μM) +GluC (0.66 μg)

Observed Mass (Da)	Theoretical Mass (Da)	Position in α-syn sequence
14502.48	14502.16	1–140
12396.82	12396.70	21–140
11554.90	11554.74	29–140
9565.30	9564.70	29–123

Ac1–122$_f$ (40 μM) +GluC (3.33 μg)

Observed Mass (Da)	Theoretical Mass (Da)	Position in α-syn sequence
12383.34	12383.00	1–122
10875.48	10875.21	14–122
10276.71	10277.54	21–122
9435.83	9435.58	29–122

Ac1–122$_f$ (40 μM) +GluC (0.66 μg)

Observed Mass (Da)	Theoretical Mass (Da)	Position in α-syn sequence
12383.24	12383.00	1–122
10875.50	10875.21	14–122
9435.72	9435.58	29–122

Ac1–103$_f$ (40 μM) +GluC (3.33 μg)

Observed Mass (Da)	Theoretical Mass (Da)	Position in α-syn sequence
10346.08	10345.86	1–103
8240.72	8240.41	21–103
7398.68	7398.44	29–103

Ac1–103$_f$ (40 μM) +GluC (0.66 μg)

Observed Mass (Da)	Theoretical Mass (Da)	Position in α-syn sequence
10346.01	10345.86	1–103
7398.53	7398.44	29–103

Table S3. CryoEM data collection, structure determination, and model statistics.

	Ac1–140	**Ac1–122**	**Ac1–103**
Data collection			
Magnification	130,000*x*	130,000*x*	130,000*x*
Defocus range (μm)	−0.8 to −1.8	−0.8 to −1.8	−0.8 to −1.8
Voltage (kV)	300	300	300
Camera	Gatan K2 Summit	Gatan K2 Summit	Gatan K2 Summit
Microscope	Titan Krios	Titan Krios	Titan Krios
Exposure time (s/frame)	0.2	0.2	0.2
Number of frames	50	50	50
Total dose ($e^-/Å^2$)	69	69	69
Pixel size (Å)	1.06	1.06	1.06
Reconstruction			
Micrographs selected	429	322	612
Manually picked segments	12,132	10,202	15,504
Box size (pixel)	200	200	200
Inter-box distance (Å)	29.4	29.4	29.4
Particles extracted	183,065	107,071	158,687
Particles after Class2D	182,562	106,940	152,261
Particles after Class3D	18,397	48,236	37,364
Final resolution (Å)	2.8	3.0	3.4
Map sharpening B-factor ($e^-/Å^2$)	−80	−80	−150
Helical rise (Å)	2.4	2.4	2.4
Helical twist (°)	179.643	179.473	179.321
Atomic model			
Number of protein residues	610	590	600
Ramachandran plot values			
Most favored (%)	79.66	87.72	65.52
Allowed (%)	18.64	12.28	34.48
Outliers (%)	1.69	0.00	0.00
Rotamer outliers	0.00	2.44	14.88
r.m.s.d Bond lengths (Å)	0.011	0.010	0.011
r.m.s.d Bond angles (°)	1.119	1.064	1.444
Clashscore	11.87	12.48	27.62
Map CC	0.79	0.79	0.75

Figure S1

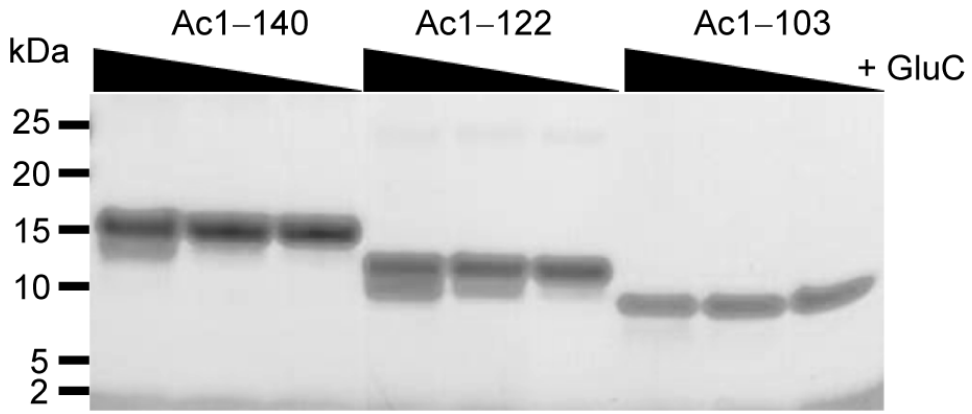

Figure S1. Degradation of Ac1–140, Ac1–122 and Ac1–103 fibrils by GluC. SDS-PAGE (4–12%) of fibrils (50 µM) incubated with GluC (3.33, 0.66 and 0.33 µg) for 20 h at 37 °C. Samples (30 µL + 10 µL LDS loading buffer) after boiling for 15 min were visualized by coomassie.

Figure S2

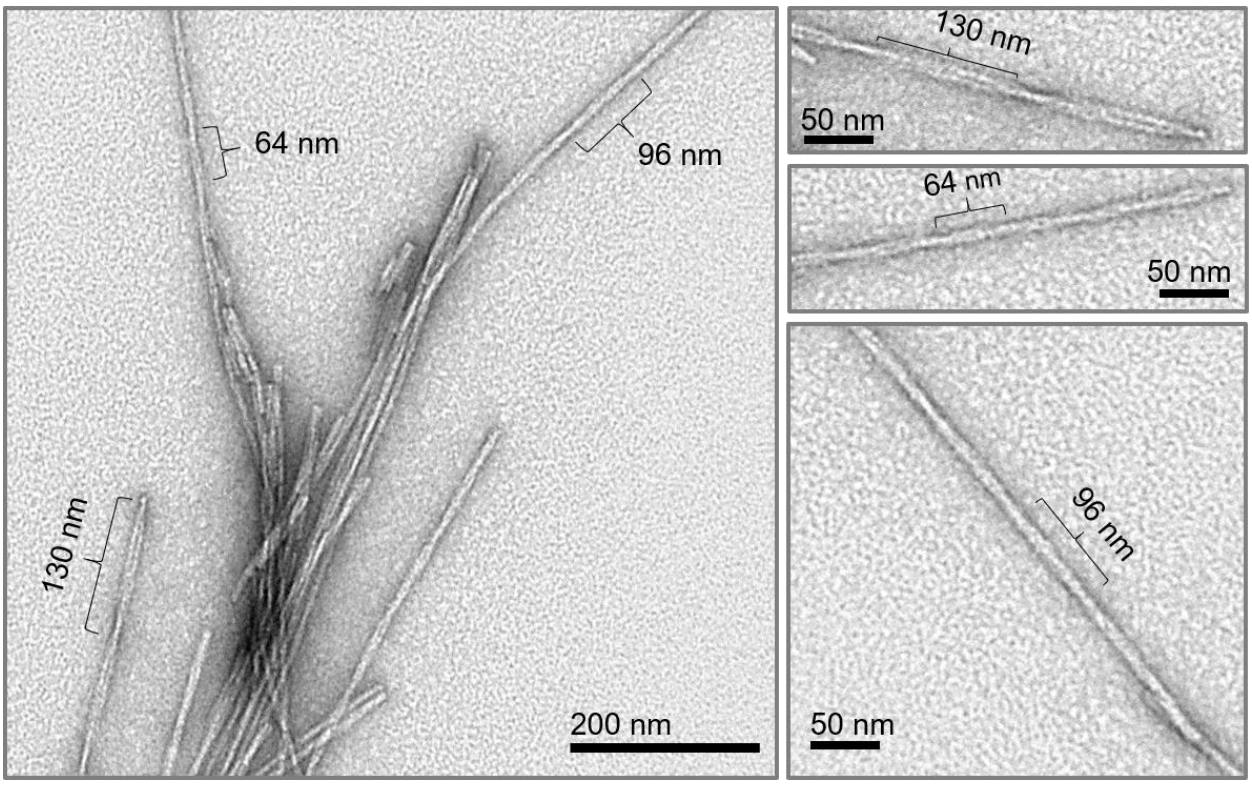

Figure S2. Negative stain TEM images of Ac1–103 fibrils formed at pH 7.4. Highlighted on one micrograph are the three distinct populations of fibrils with varying half pitches (64, 96, and 130 nm).

Figure S3

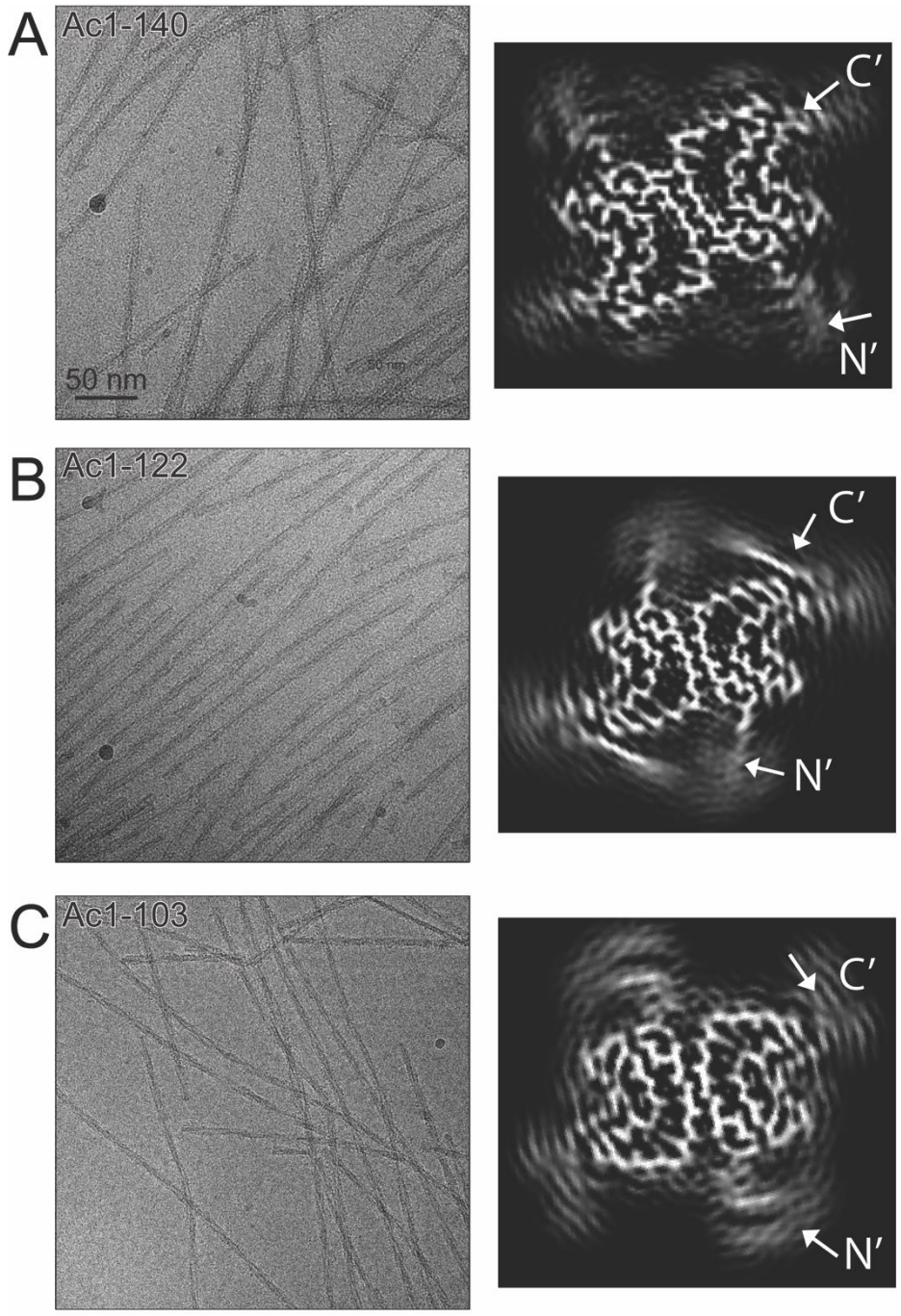

Figure S3. CryoEM micrographs and cross-sections of 3D reconstructions of the α-syn fibrils. (**A**) Ac 1–140, (**B**) Ac 1–122, and (**C**) Ac1–103. In each panel, left: a representative cryoEM micrograph; right: a cross-section along the *x-y* plane of the density map of the 3D reconstruction. The cross-sections (4 pixels in thickness) clearly reveal zigzagged densities featured by the β-strands of the α-syn fibrils. The resolvable N- and C-terminal regions of the α-syn fibrils are labelled.

Figure S4

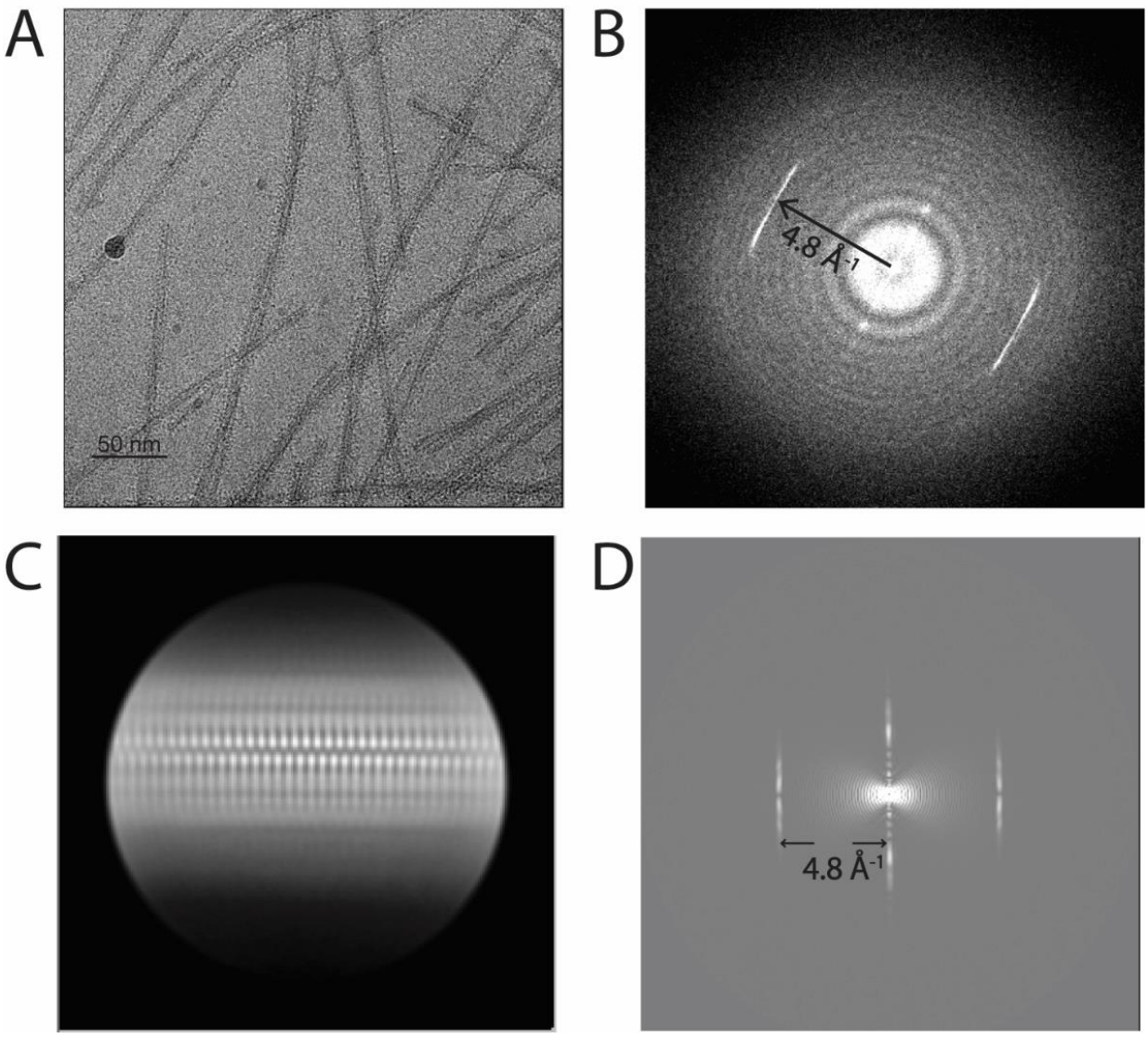

Figure S4. Helical parameter estimation. (**A**) A representative cryoEM micrograph of Ac1–140. (**B**) The power spectrum of a selected micrograph in **A**. The layer lines (show with an arrow) corresponding to the helical rise. (**C**) A typical 2D class average of α-syn fibrils showing a staggered conformation between two protofibrils. (**D**) The layer lines calculated from a 2D class average that correspond to the helical rise are consistent with the rise calculated from power spectrum in **B**.

Figure S5

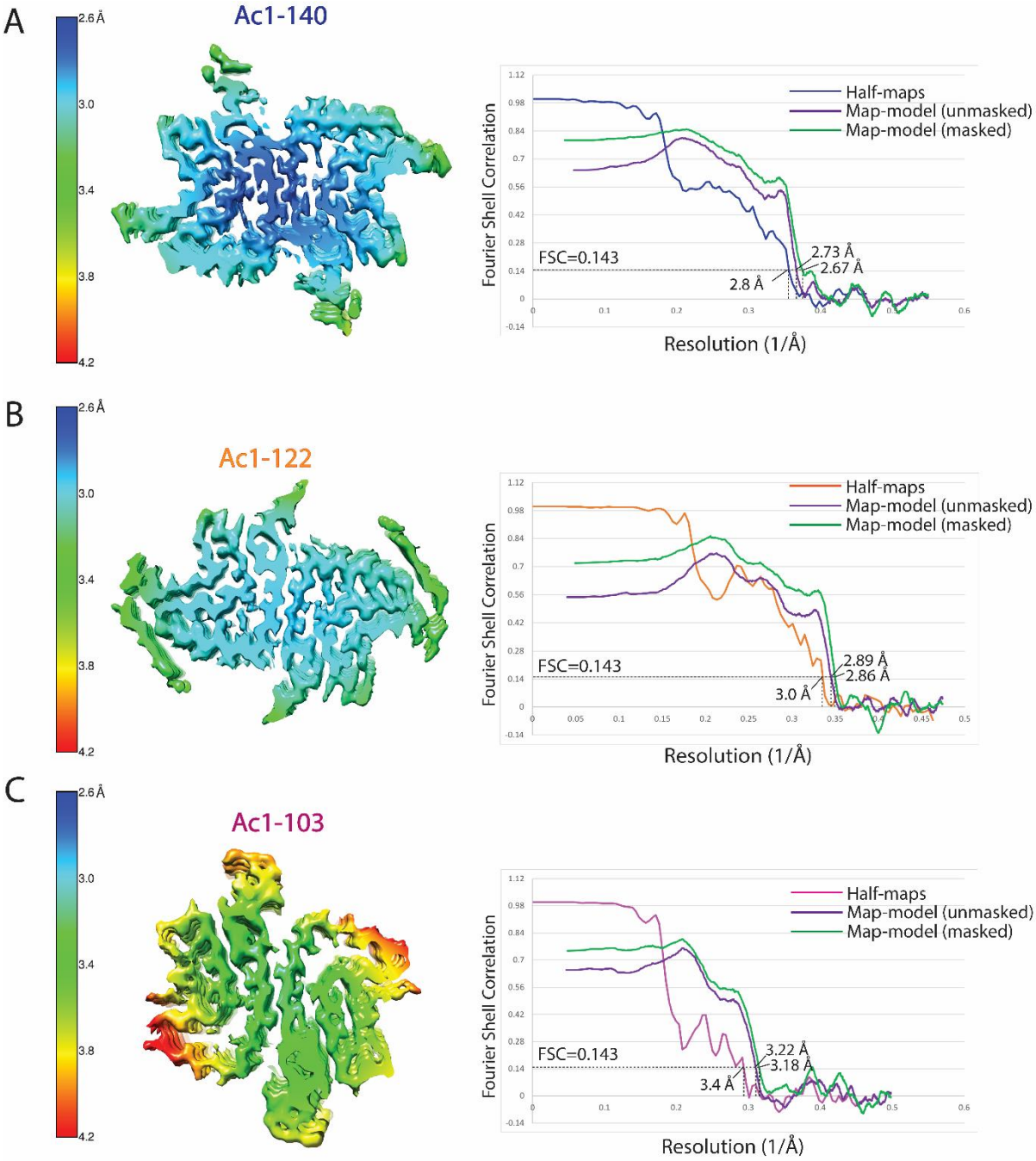

Figure S5. Local resolution estimation and gold-standard Fourier Shell Correlation (FSC) curves for resolution estimation. Local resolution maps (left panels) of α-syn fibrils (**A**) Ac1–140, (**B**) Ac1–122 and (**C**) Ac1–103, showing that the highest resolution is at the interface region between the two protofilaments. An FSC cutoff value at 0.143 was used to estimate the final resolution and the map-model correlations for α-syn fibrils (right panels). The overall resolution is 2.8, 3.0, and 3.4 Å for Ac1–140, Ac1–122, and Ac1–103, respectively.

Figure S6

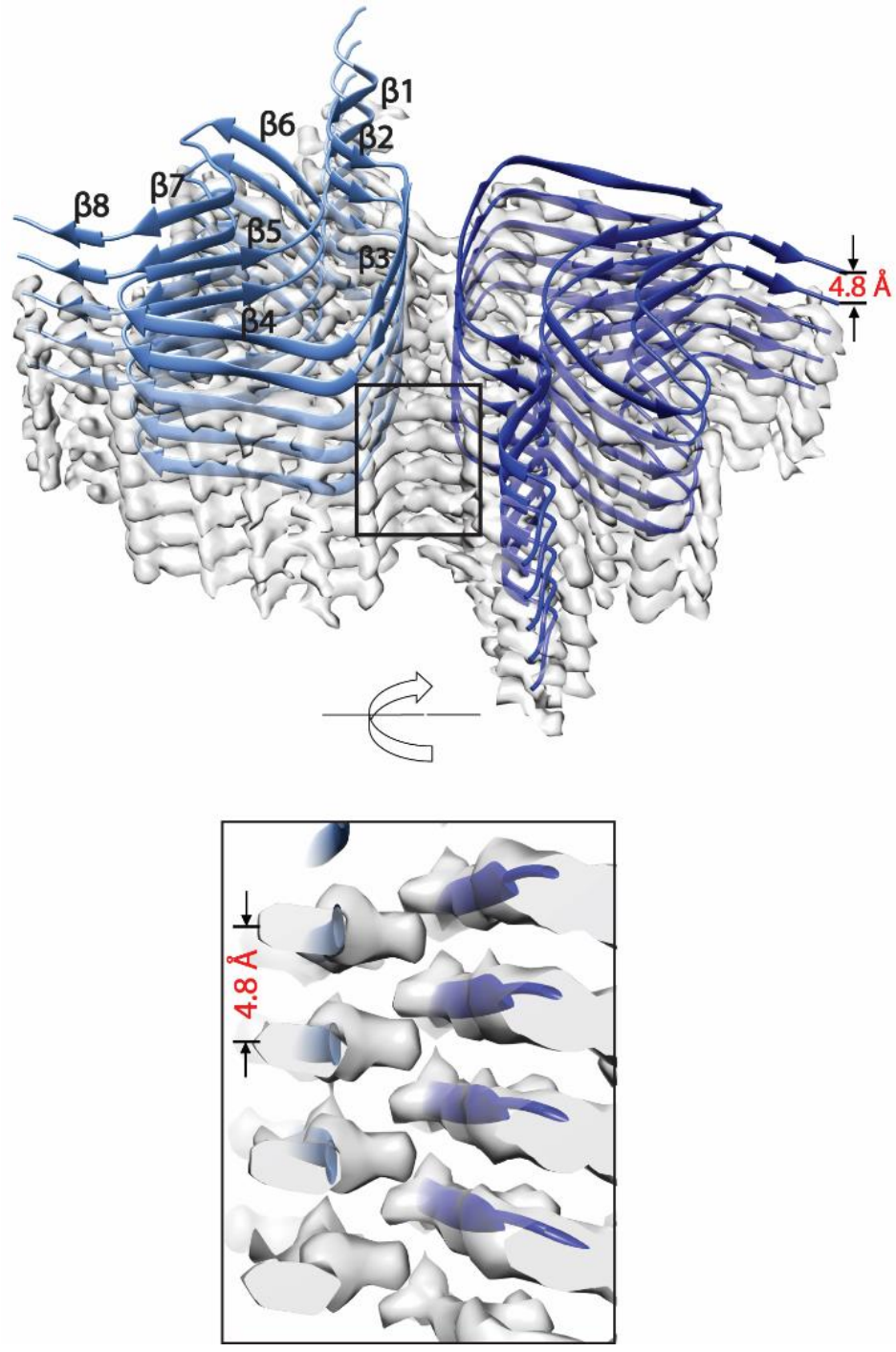

Figure S6. A tilted view of the α-syn density map shows the distribution of β-strands in a single protofilament. The distance between two stacked β-sheets is as indicated. Shown at the bottom is the side view of the density map with the helical rise labeled.

Figure S7

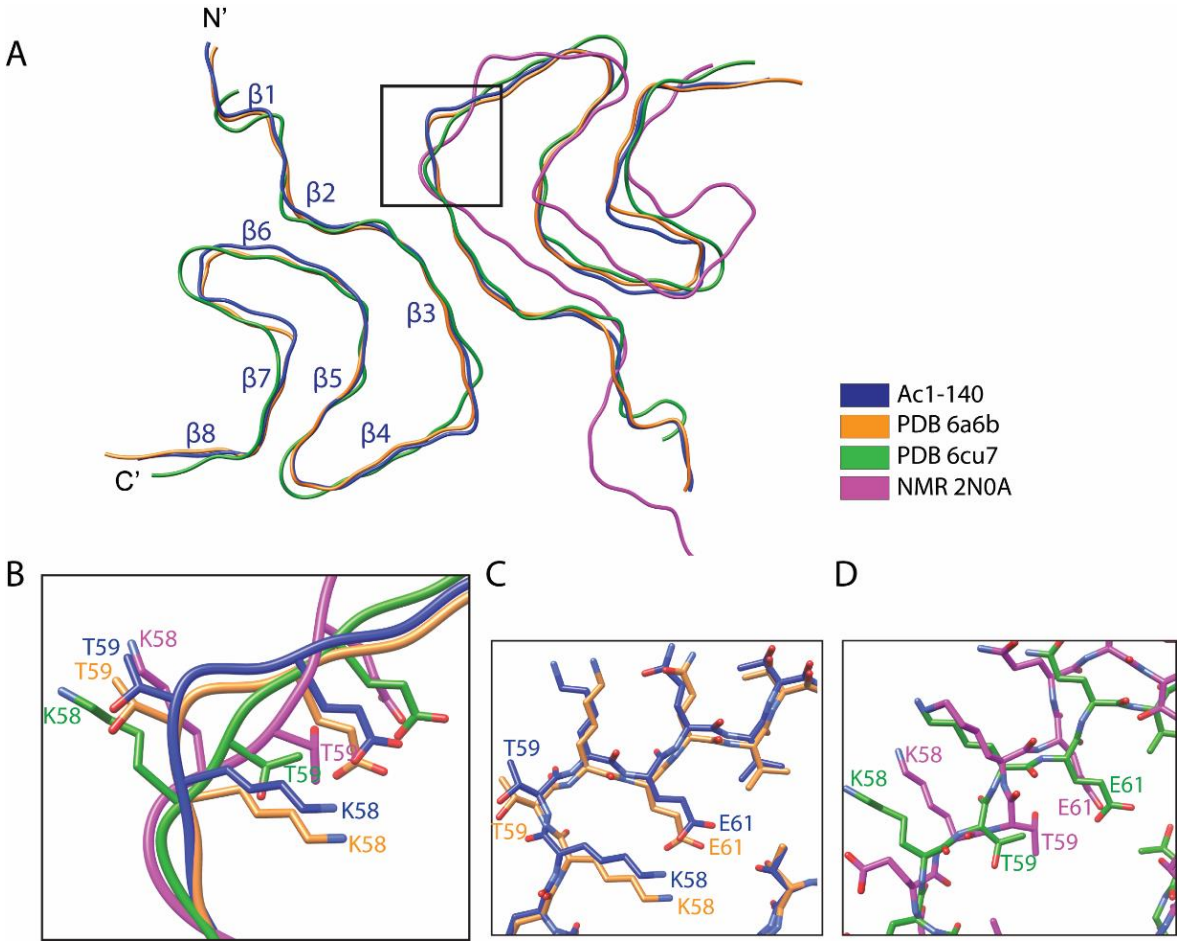

Figure S7. Comparison of the cryoEM structures of the full length (1–140) α-syn fibril with the solid-state NMR protofilament structure. (**A**) Backbone overlay of the Ac1–140 (blue) structure determined in this work compared with the other full length α-syn fibril structures including PDB 6A6B (gold, overall RMSD: 0.75 Å), PDB 6CU7 (green, overall RMSD: 2.11 Å), and the ssNMR structure PDB 2N0A (magenta, overall RMSD: 6.08 Å). (**B**) Residues K58–T59 has the same conformation in both Ac1–140 (blue) and PDB 6A6B (gold) that forms a salt bridge (**C**) which are both N-terminally acetylated, whereas in both the non-acetylated forms (PDB 6CU7, green; PDB 2N0A, magenta), the salt bridge is broken between K58–E61 because K58 is flipped outward (**D**).

Figure S8

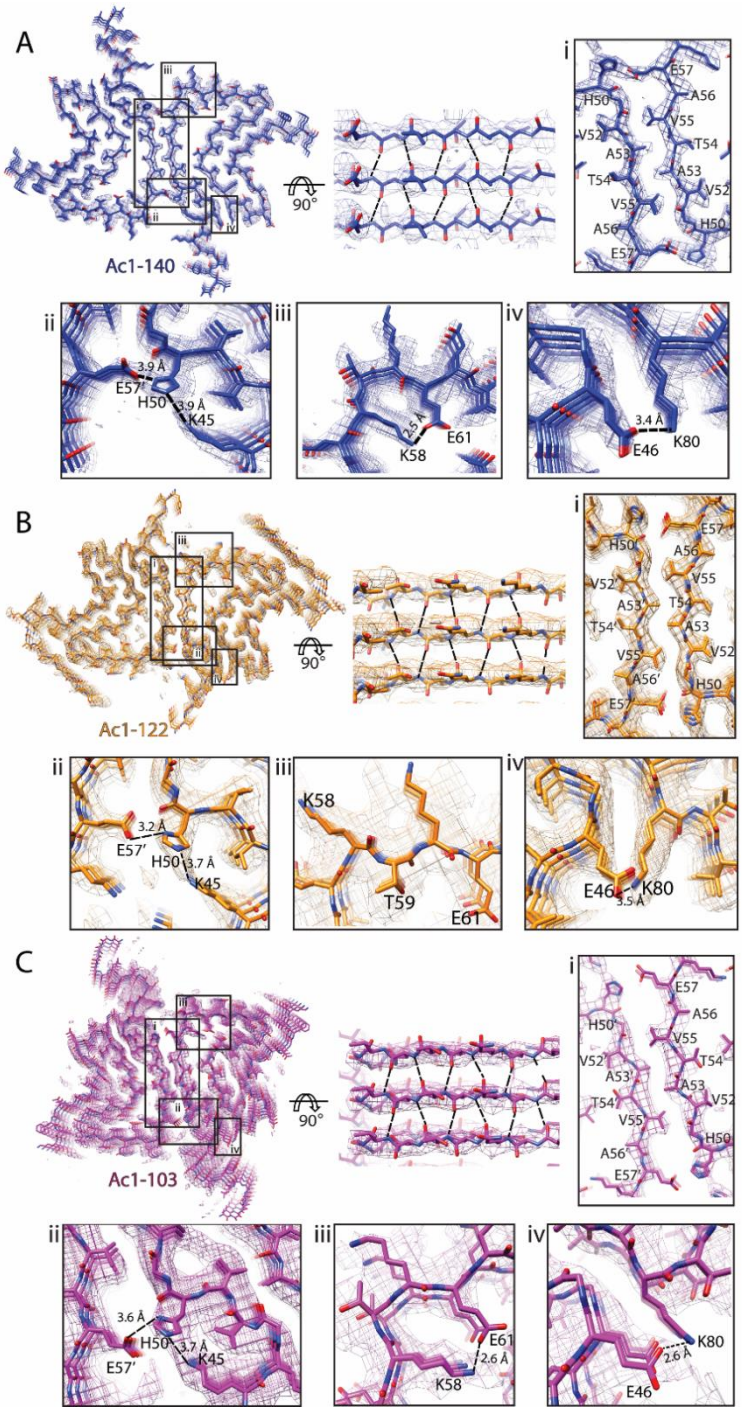

Figure S8. Side chain interactions in the α-syn fibril structures. (**A-C**) A top view of α-syn fibril Ac1–140 (**A**), Ac1–122 (**B**) and Ac1–103 (**C**) with two protofilaments. The density maps of Ac1–140 (blue), Ac1–122 (gold) and Ac1–103 (magenta) are shown as mesh surfaces. Intra-protofilament hydrogen bonds and inter-protofilament interactions are shown in black dashed lines. The interface between two protofilament (**A**–**C**, **i**) comprises residues H50–E57. Symbol ' represents residues on the opposing subunit. Electrostatic interactions among E57'–H50–K45 (**A**–**C**) are indicated in box ii. Salt bridges formed by K58–E61 (**A** and **C**) are shown in box iii, while E46–K80 (**A** and **C**) are indicated in box iv.

Figure S9

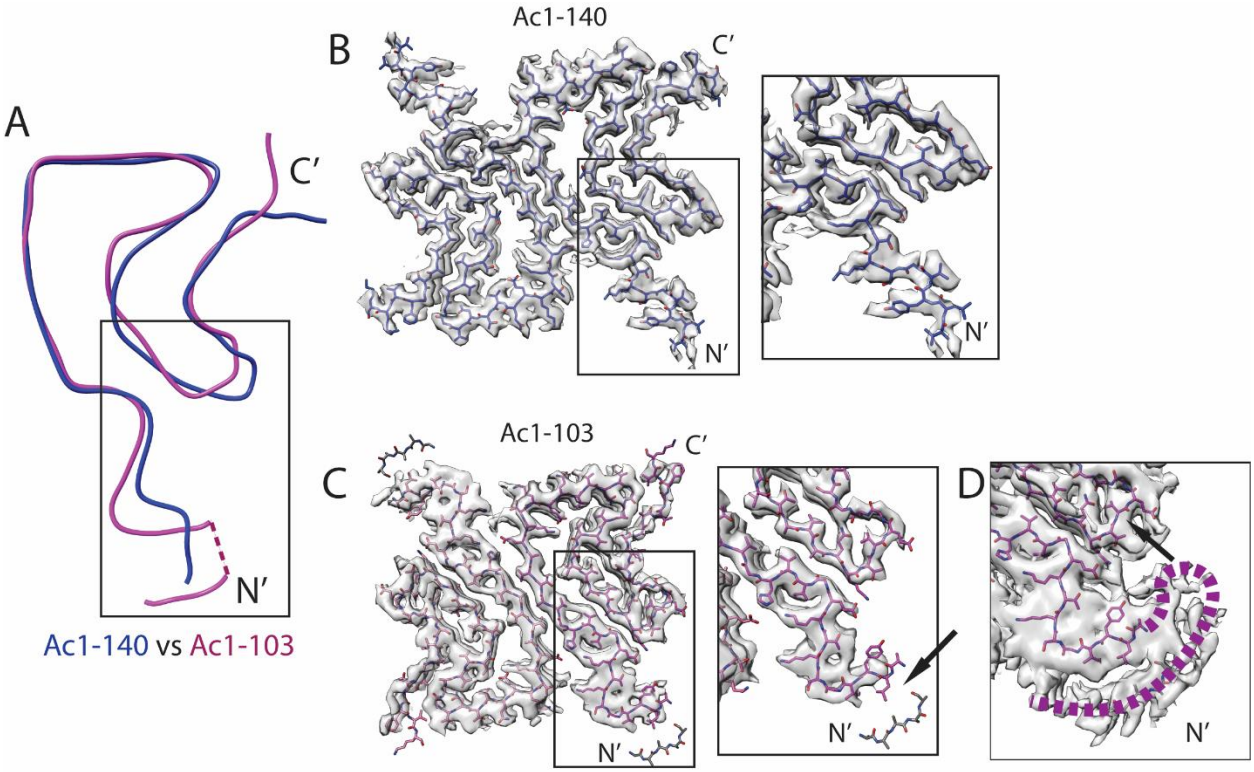

Figure S9. An expanded view of the EM density comparing the N-terminal regions of Ac1–103 and Ac1–140. (**A**) Backbone overlays highlight differences (indicated by box) on the N-terminal region between Ac1–103 and Ac1–140. (**B**) Left panel: Density map of Ac1–140 with the model fitted in and the N- and C-termini as indicated. Right panel: An expanded view. (**C**) Left panel: Density map of Ac1–103 with the model fitted in and the N- and C-termini as indicated. Right panel: An expanded view. Density on the N-terminus of Ac1-103 that can be well resolved, whereas the region that can not be reliable modeled is indicated by arrow. (**D**) Density observed on the N-terminal region of Ac1–103 through adjustment of display thresthold. Dashed line in magenta illustrates the possible architecture of the N-terminus of Ac1–103, indicating a close proximity to the turn region (between β6 and β7 strands, indicated by arrow).